CrossMark

Evaluation of High Temperature Corrosion in Simulated Waste Incinerator Environments

J. A. Alcántara-Cárdenas[1,2] · **A. Ramirez-Lopez**[2] ·
J. F. Chávez-Alcalá[1] · **M. Sanchez-Pastén**[1]

Abstract In this study, high temperature reactions of Fe–Cr alloys at 500 and 600 °C were investigated using an atmosphere of N_2–O_2 8 vol% with 220 vppm HCl, 360 vppm H_2O and 200 vppm SO_2; moreover the following aggressive salts were placed in the inlet: KCl and $ZnCl_2$. The salts were placed in the inlet to promote corrosion and increase the chemical reaction. These salts were applied to the alloys via discontinuous exposures. The corrosion products were characterized using thermo-gravimetric analysis, scanning electron microscopy and X-ray diffraction.The species identified in the corrosion products were: Cr_2O_3, Cr_2O $(Fe_{0.6}Cr_{0.4})_2O_3$, K_2CrO_4, $(Cr, Fe)_2O_3$, Fe–Cr, KCl, $ZnCl_2$, FeOOH, σ-FeCrMo and Fe_2O_3. The presence of Mo, Al and Si was not significant and there was no evidence of chemical reaction of these elements. The most active elements were the Fe and Cr in the metal base. The Cr presence was beneficial against corrosion; this element decelerated the corrosion process due to the formation of protective oxide scales over the surfaces exposed at 500 °C and even more notable at 600 °C; as it was observed in the thermo-gravimetric analysis increasing mass loss. The steel with the best performance was alloy Fe9Cr3AlSi3Mo, due to the effect of the protective oxides inclusive in presence of the aggressive salts.

Keywords Waste incinerator · Chemical reactions · Aggressive salts · Oxide formation

✉ J. A. Alcántara-Cárdenas
jaac_beto@hotmail.com

✉ A. Ramirez-Lopez
adan.ramirez@itam.mx; adaralo@starmedia.com

1   Department of Engineering in Metallurgy and Materials, Instituto Politecnico Nacional (ESIQIE-IPN), CP 07738 Mexico City, Mexico

2   Department of Industrial Engineering, Instituto Tecnologico Autonomo de Mexico (ITAM), CP 01080 Mexico City, Mexico

Introduction

The phenomenon of corrosion in waste incinerators is influenced by different factors such as pressure, temperature, the chemical composition of the gases during combustion and the different salts condensed on the walls in addition to superheats and humidity during operating. The temperature conditions inside the waste incinerators are between 300 and 600 °C; depending on the reactor. Nevertheless these conditions increase the aggressiveness of the atmosphere. Thus, it is very important to know the performance of the materials used to build these industrial devices in order to guarantee the equipment integrity.

The specific Composition of the gases (N_2, HCl, SO_2, CO, O_2 and H_2O) and the salt deposits are always variable due to the heterogeneity of the wastes burned, however many chlorides and sulphates were identified over the samples [1]. The reaction between alkaline salts and water on small quantities in addition to the thermodynamic conditions of the system causes the breakdown of the protective scale of Cr_2O_3 in the steel [2, 3]. Moreover, many of the corrosion products are porous, weak and not protective oxides and chromates [3, 4].

The effect of some alloying elements such as Mo in stainless steels is not significant because it does not protect the steel against corrosion; this fact has been reported in previous laboratory studies [5], and during real waste incinerators operation [6]. The addition of Al and Si to the stainless steel has shown effectiveness to form protective oxide layers against corrosion due to the products formed are thermodynamic stable at elevated temperatures inhibiting the chemical reactions and avoiding the mass loss. Nevertheless this could not be observed during testing, perhaps because Cr was the dominant element in the metal base composition.

Experimental Procedures

The chemical composition of the four stainless steels tested during the corrosion experiments is shown in Table 1. The Fe–Cr alloys were prepared by induction and melting using commercial low carbon steel. Then the alloying elements were melted with; after this, the samples were decarburized and de-oxided in an induction furnace. Then the alloys were cast in 150×150 mm square ingots. Longitudinal bars from the middle of the squared section were cut and thermo-mechanically processed to refine the microstructure and provide ductility even with the presence of the precipitates formed. After that the coupons were cut with dimensions

Table 1 Alloys composition (mass%), every alloy is a steel based with 0.08C

ID	Alloy	Cr	Al	Mo	Si	Fe
1	Fe9Cr2.5AlSi5Mo	9	2.5	5	2.5	80.92
2	Fe9Cr2.5AlSi3Mo	9	2.5	3	2.5	82.92
3	Fe9Cr1.5AlSi3Mo	9	1.5	3	1.5	84.92
4	Fe9Cr3AlSi3Mo	9	3	3	3	81.92

$10 \times 10 \times 2$ mm. The samples were prepared using SiC sandpaper to 600-grit and then cleaned, using acetone and then ethanol, in an ultrasonic bath to be finally weighed.

Isothermal time-resolved exposures were carried out in N_2–O_2 8 vol% 220 ppm HCl 360 ppm H_2O 200 ppm SO_2 at 500 and 600 °C using a mixture of salts in the reactor inlet with the following composition: 16 mg of $ZnCl_2$ and KCl during a period of 300 h inside the furnace which was hermetically sealed. A SiO_2-quartz glass tube with an inner diameter of 50 mm was placed in the inlet and the injection flux used was 4 ml/s. This experimental environment was selected to reproduce some aggressive mixes inside incinerators, although other authors [7] have worked with other specific atmospheres due to the different chemical composition of their wastes.

The test set-up is shown in Fig. 1. The KCl and $ZnCl_2$ were placed in the inlet of the furnace in order to simulate the aggressive environment. The purpose is that these salts were foundry and mixed with the gas mixture and then driven towards the metal samples. The gas mixture was composed with very aggressive substances such as SO_2, HCl and H_2O which are frequently found inside incinerators. In Fig. 1 the O_2 and SO_2 gases are induced to the furnace directly but the aggressive agents; H_2O and HCl are mixed with (N_2) to be driven towards the furnace. The salts were
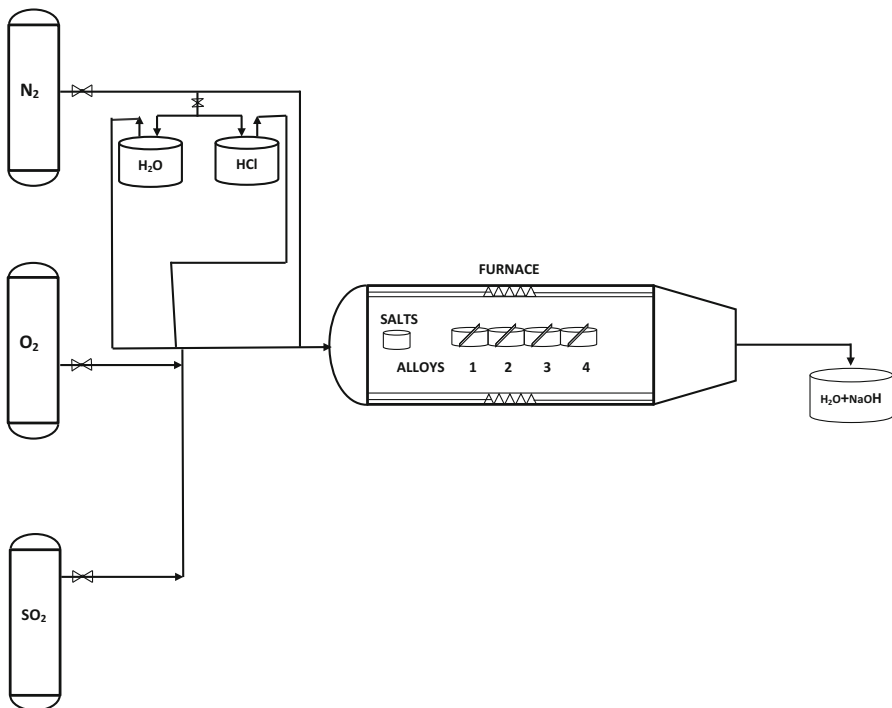
Fig. 1 Experimental setup for exposures using a horizontal silica furnace

placed near the inlet furnace to be conducted along the sample surface profiting the convection force of the fluid flow.

The samples were exposed discontinuously in periods of 1, 3, 10, 30, 100 and 300 h. These periods of time were selected to study the incubation period and are consider as long enough to reach isothermal conditions inside the furnace. The samples were weighed at the end of each testing period to measure the mass loss. The corrosion products were removed by chemical etching in a $KMnO_4$ solution at 80 °C; and then cleaned with NaOH in an ultrasonic bath once again [8]. After, the samples were taken out the furnace and unclasped in bakelite and then polished using alcohol to avoid post-oxidation; and a very fine electro-deposition of Au–Pd
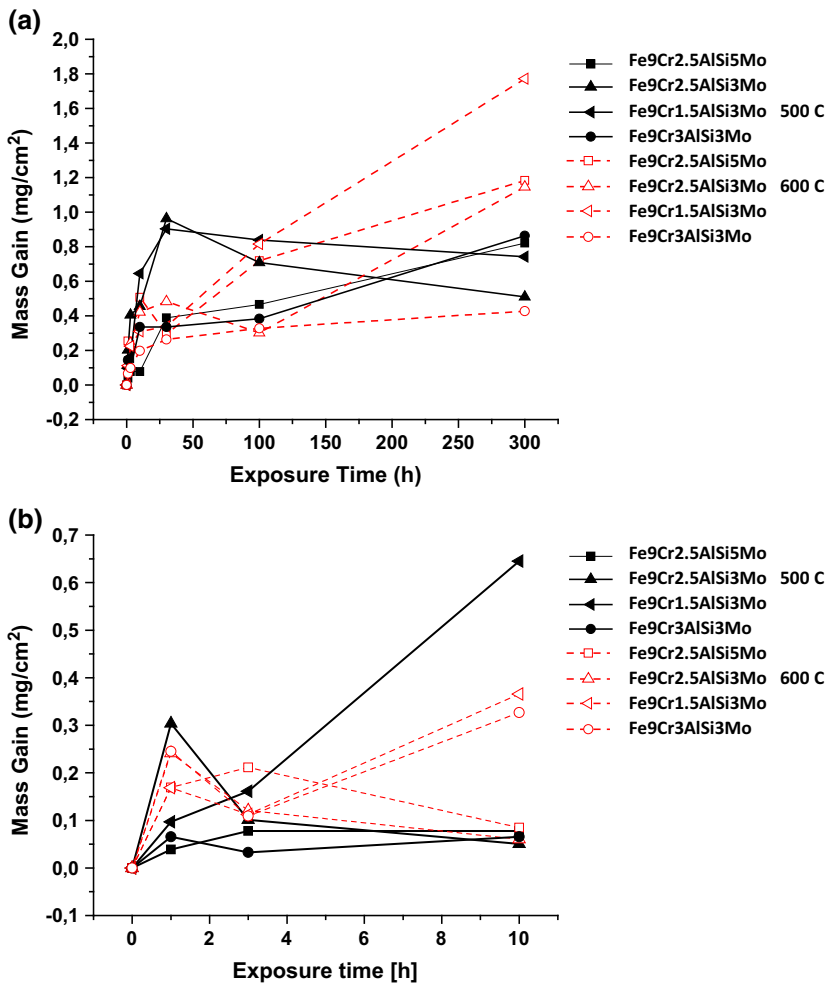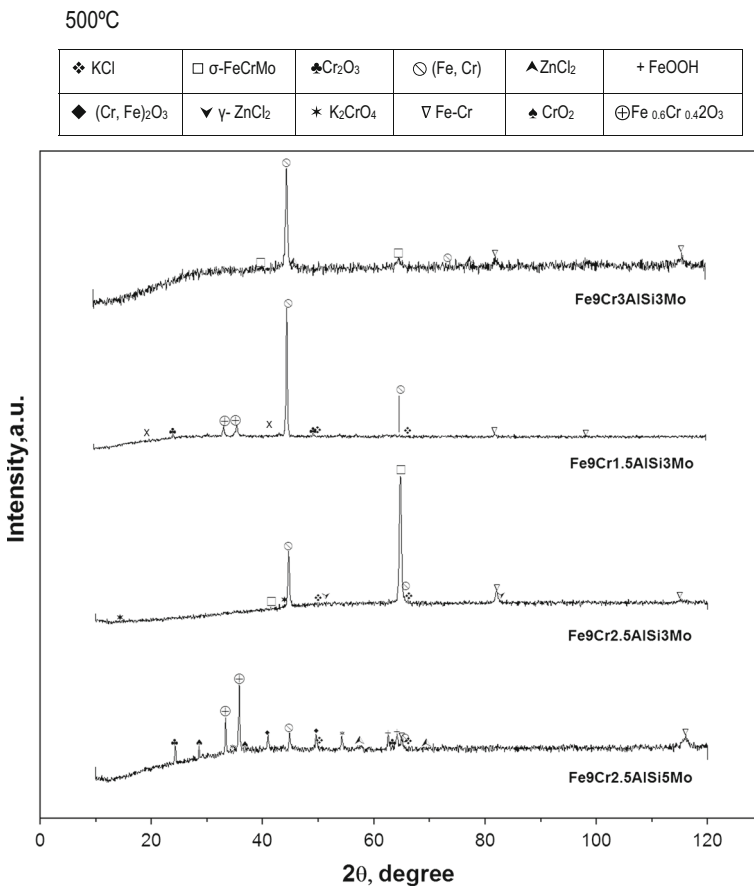

Fig. 2 Thermo-gravimetric analysis showing mass loss as a function of exposure time for the alloys studied in N_2–O_2 8 vol% 220 vppm HCl 360 vppm H_2O 200 vppm SO_2 environment at 500 and 600 °C in the presence of KCl and ZnCl. **a** 300 h long exposition period. **b** 10 h short exposition period

was placed over the sample surface to improve conductivity, then it was possible to characterize the surface and corrosion products using a scanning electron microscope (HR-SEM), Jeol 6701F, with EDS using an acceleration voltage of 20 kV and X-ray diffraction (XRD) with a Brucker D8 Focus in order to know and quantify the chemical composition of the products.

Thermo-gravimetric Measurements

The thermo-gravimetric curves for the four alloys in N_2–O_2 8 vol% 220 vppm HCl 360 vppm H_2O 200 vppm SO_2 environment at 500 and 600 °C in presence of KCl and $ZnCl_2$ are shown in Fig. 2a. Here it can appreciated that the alloy Fe9Cr2.5AlSi5Mo at 500 °C after 10 h of exposure shown a notable increment in mass loss, but after 30 h the increment was slower approaching a logarithmic curve

500ºC

❖ KCl	□ σ-FeCrMo	♣ Cr_2O_3	◌ (Fe, Cr)	▲ $ZnCl_2$	+ FeOOH
◆ $(Cr, Fe)_2O_3$	▼ γ- $ZnCl_2$	✳ K_2CrO_4	▽ Fe-Cr	♠ CrO_2	⊕ $Fe_{0.6}Cr_{0.42}O_3$

Fig. 3 XRD patterns of oxide scales formed on Fe–Cr alloys corroded during 300 h in N_2–O_2 8 vol% 220 vppm HCl 360 vppm H_2O 200vppm SO_2 environment at 500 °C in the presence of KCl and ZnCl

which indicate that the oxide was stabilized and that the incubation period has been finished. While at 600 °C a decrement on the mass loss was observed for a time of 10 h and for 30 h the increment was constant until the end of the test. Furthermore the alloy Fe9Cr2.5AlSi3Mo had a notorious increment before 30 h and after that there was a slight decrement; however at the end of the test a decrement was also observed at 500 °C, but the mass loss remains without change for long exposure periods. This alloy behaved similarly at the beginning for testing at 600 °C; but after 100 h there was a constant increasing linear trend indicating that the mass loss also continues. In this case the increment on the atmospheric temperature promoted a continuous attack over the sample. The alloy Fe9Cr1.5AlSi3Mo at 500 °C showed an accelerated mass loss at the beginning of the test; here it was a parabolic behavior but after 30 h there was a decrement until the end of test, while at 600 °C the incubation period was also short, after 30 h it was a constant increment on the mass loss until the end. Finally the alloy Fe9Cr3AlSi3Mo had a similar logarithmic form over 100 h for both temperatures. But the steel maintained a logarithmic trend for long exposition times at 600 °C while at 500 °C a parabolic trend was obtained until
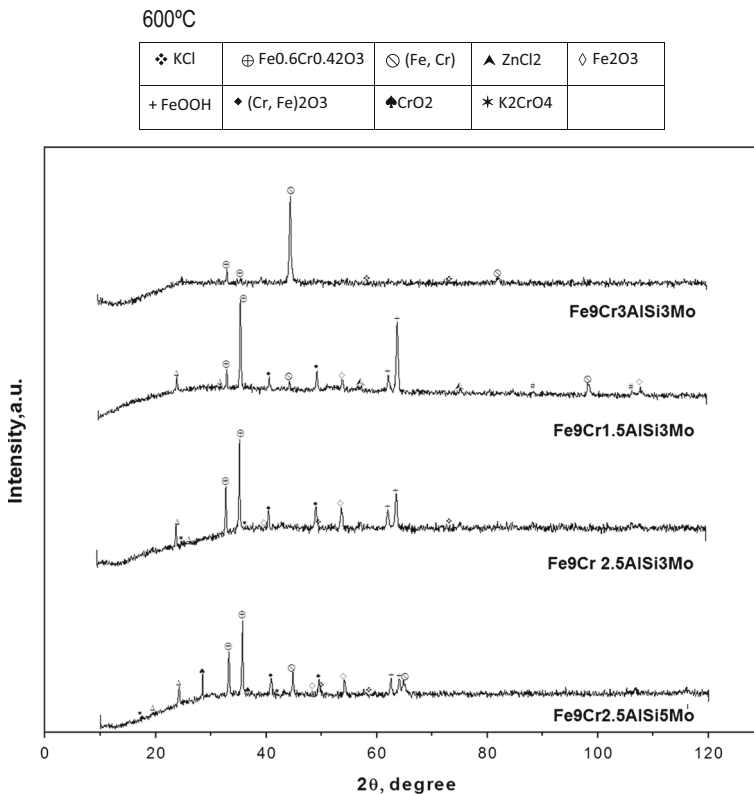
Fig. 4 XRD patterns of oxide scales formed on Fe–Cr alloys corroded during 300 h in N_2–O_2 8 vol% 220 vppm HCl 360 vppm H_2O 200 vppm SO_2 environment at 600 °C in the presence of KCl and ZnCl

the end of the test. According with these facts, this alloy had the best corrosion resistance because it was with the lowest mass loss.

Figure 2b is a close up of its previous; here it is possible to verify the behavior of each alloy during the incubation period. There is an initial increment on mass loss for all the alloys, which indicates that the oxidation has begun. Nevertheless there is a decrement after 3 h due to the oxide scale formed but sometimes is also removed from the sample surface due to the fluid flow; so the corrosion phenomena continues. Finally for longer periods between 3 and 10 h the mass loss continues increasing but the curve slopes are moderates, evidencing that the corrosion phenomena was stabilized.

Scale Composition by EDX

The chemical composition of the oxides formed for all the alloys are shown in Figs. 3 and 4 at 500 and 600 °C respectively, in the XRD analysis of alloy Fe9Cr2.5AlSi5Mo at 500 °C the presence of the following species was detected: Cr_2O_3, CrO_2, $(Fe_{0.6}Cr_{0.4})_2O_3$ higher intensity (Cr, Fe) $2O_3$, (Fe, Cr) Iron chrome, KCl, $ZnCl_2$ both chlorides with low intensity. Moreover the presence of FeOOH was also observed in the mapping with SEM; nevertheless this is not a corrosion product; it is formed due to the reaction with humidity in the external environment. Here a thicker scale was formed as a consequence of the corrosion process which was not stopped and major quantities of different and heterogeneous products were also formed.

XRD analysis for the alloy Fe9Cr2.5AlSi3Mo at 500 °C, shown the presence of the following compounds: potassium, chromate K_2CrO_4, KCl, γ-$ZnCl_2$ with a light intensity and Fe–Cr and during searching XRD the stainless steel of the metal base has also found. No significant peaks were identified for oxides of Fe, Cr, Si, Mo or Al. Thus it is possible to affirm that under the experimental conditions this alloy was not suffering a severe reaction with alkaline salts inside the simulated atmosphere.

The following compounds were identified for the alloy Fe9Cr1.5AlSi3Mo: chromium oxide Cr_2O_3, $(Fe0.6Cr0.4)_2O_3$ chromium and iron oxide, as well as potassium chloride KCl (Fe–Cr). Here the oxide scale was very thin and the metal base was also detected; although, this thin scale was effective enough to avoid partially the corrosion process and inhibit other chemical reactions. This fact is confirmed because the most abundant elements correspond to the compounds identified that formed the protective oxides. Although potassium chloride was also detected in this sample as a result of the chemical reaction with the salt in the inlet, the peaks were low due to almost all this product continued reacting with the metal surface and the atmosphere. In Fig. 3, the products formed for the alloy Fe9Cr3AlSi3Mo were the following: σ-FeCrMo, $ZnCl_2$ and (Fe–Cr) these two appear because are parts of the metal base and the intensity of the $ZnCl_2$ peaks is very low in comparison with the rest of the products.

Figure 4 shows the XRD analysis for 4 alloys tested at 600 °C. The peaks identified for the alloy Fe9Cr2.5AlSi5Mo corresponded to the following products: K_2CrO_4 potassium chromate, chromium oxide CrO_2 $(Fe0.6Cr0.4)_2O_3$ oxide of iron

and chromium, $(Cr, Fe)_2O_3$ chromium and iron oxide, as Fe_2O_3 hematite iron oxide, potassium chloride KCl, confirming that the test atmosphere promoted oxidation, mainly Fe and Cr; so the alloy was reactive under the testing conditions. Here the lowest intensity peaks correspond to K_2CrO_4 and KCl. The alloy was again very active and many products were formed. The products identified during XRD analysis for alloy Fe9Cr2.5AlSi3Mo were the following: K_2CrO_4 potassium chromate $(Fe_{0.6}Cr_{0.4})_2O_3$ iron and chromium oxide, iron oxide Fe_2O_3 as synthetic hematite $(Cr, Fe)_2O_3$ chromium and iron oxide, potassium chloride KCl and FeOOH iron oxide hydroxide. Here the compounds formed indicate that the surface was also reactive with the atmosphere; the K_2CrO_4 and KCl had the lowest intensity. The XRD analysis on the surface of alloy Fe9Cr1.5AlSi3Mo at 600 °C identified the following oxides: $(Fe_{0.6}Cr_{0.4})_2O_3$ oxide of iron and chromium $(Cr, Fe)_2O_3$ chromium and iron oxide, iron oxide Fe_2O_3 as synthetic hematite, zinc chloride $ZnCl_2$, FeOOH hydroxide. More chemical reactions were occurring and more products were identified in this sample. In contrasts only a few products were identified for the alloy Fe9Cr3AlSi3Mo after testing; only $(Fe_{0.6}Cr_{0.4})_2O_3$ and KCl were formed. The facts mentioned above evidence that the alloys are reactive under the aggressive atmospheres within the furnace and therefore there is a significant amount of oxides of which only some of them are protective.

Figure 5 shows the mass loss for the four alloys. The most aggressive temperature for alloys Fe9Cr2.5AlSi5Mo and Fe9Cr2.5AlSi3Mo was 600 °C; here it is possible to appreciate that the increment on the temperature generates a major mass loss. Nevertheless for alloys Fe9Cr1.5AlSi3Mo and Fe9Cr3AlSi3Mo the increment on the temperature generates a moderate reduction on mass loss. Alloys Fe9Cr1.5AlSi3Mo and Fe9Cr3AlSi3Mo shown the best performance at 600 °C due to a minor number of chemical reactions occurred and because these were with the minor mass loss; in contrast alloys Fe9Cr2.5AlSi5Mo and Fe9Cr2.5AlSi3Mo had a better resistance at 500 °C.
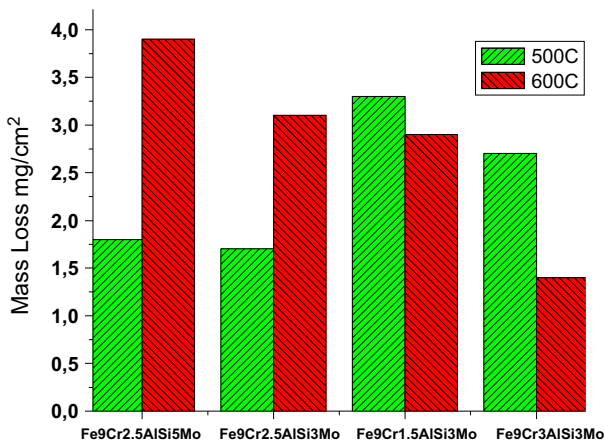

Fig. 5 Mass loss of Fe–Cr alloys in N_2–O_2 8 vol% 220 vppm HCl 360 vppm H_2O 200 vppm SO_2 environment at 500 and 600 °C in the presence of KCl and ZnCl

Figure 6a–d shows the morphology obtained of the four alloys after 300 h at 500 °C. These pictures were taken at ×2000 using a SEM. The darkness areas appreciated in Fig. 6a correspond to the metal base and the gray areas are the oxidized regions. This oxide remains over the sample surface but not cover all entire. In consequence, big areas of the metal base can continue reacting with the aggressive atmosphere and the corrosion process continues. In contrast in Fig. 6b the gray areas are bigger than in the previous and certain protection is provided to the metal base. In Fig. 6c many whiskers are displayed over the metal surface; these bigger particles are KCl or $ZnCl_2$; Whiskers are mainly composed with chromium oxides or iron oxides. Some of them form a protective scale, that avoid the corrosion reaction and in Fig. 6d the surface shows a large dark oxide scale with a minimum amount of fine particles, alkaline chlorides and Fe whiskers are also observed, moreover it is impossible to observe the metal base; it means that the scale covers entirely the metal base avoiding the corrosion process continues.

Figure 7a–d shows the morphology obtained of the four alloys after 300 h at 600 °C. Fe9Cr2.5AlSi5Mo micrograph shows the metal base and certain oxides, some whiskers and a considerable amount of polyhedral precipitates which were identified as potassium chromates after a mapping study employing a SEM. The polyhedral geometries are also amorphous and are with different sizes from 3.5 to
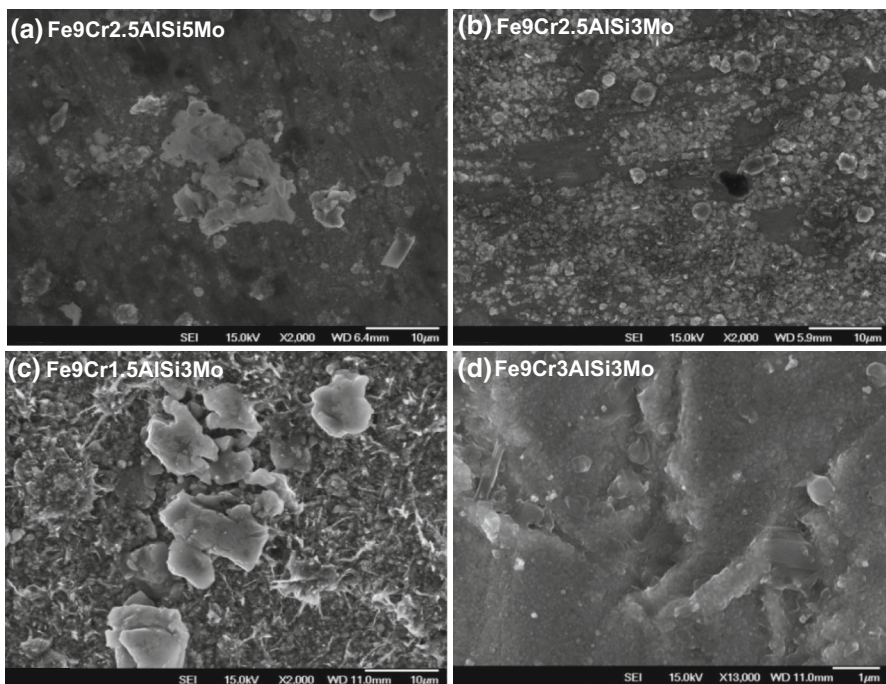
Fig. 6 Surface morphologies of the four alloys after 300 h corrosion in N_2–O_2 8 vol% 220 vppm HCl 360 vppm H_2O 200 vppm SO_2 in the presence $ZnCl_2$ and KCl at 500 °C
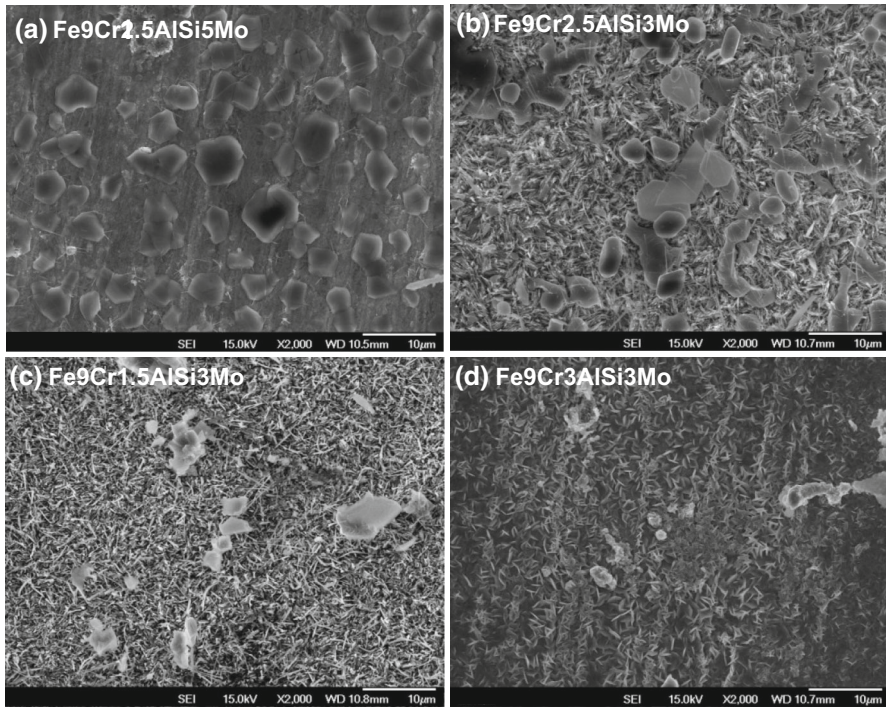
**Fig. 7** Surface morphologies of the four alloys after 300 h corrosion in N_2–O_2 8 vol% 220 vppm HCl 360 vppm H_2O 200 vppm SO_2 with addition $ZnCl_2$ and KCl at 600 °C

7.5 μm averaged diameter. These precipitates are here due to chemical reactions between the metal base and the aggressive salts added.

Figure 7b is a micrograph at ×2000 and corresponds to alloy Fe9Cr2.5AlSi3Mo. Here the dark oxide of the scale can be appreciated; moreover little whiskers and small particles surrounding globular appear with irregular sharped light color. These particles were mapped using SEM analysis and revealed that these are chromates such as K_2CrO_4. But whiskers are mainly composed with iron oxide which is weak and porous.

In Fig. 7c the surface of the alloy Fe9Cr1.5AlSi3Mo is lightly colored with polygonal particles and other irregular shapes. The surface is covered with many little whiskers and some dark areas of oxides, these whiskers can provide a partial corrosion protection over the surface; but these are not enough consolidated to avoid it.

Figure 7d correspond to the alloy Fe9Cr3AlSi3Mo, here an oxide scale is covering partially the surface; this can be observed in dark color. Here the whiskers are aligned in the same direction than sanding lines. These whiskers were nucleated separately but not growth enough to cover the sanding lines allowing the aggressive atmosphere contacted the metal base.
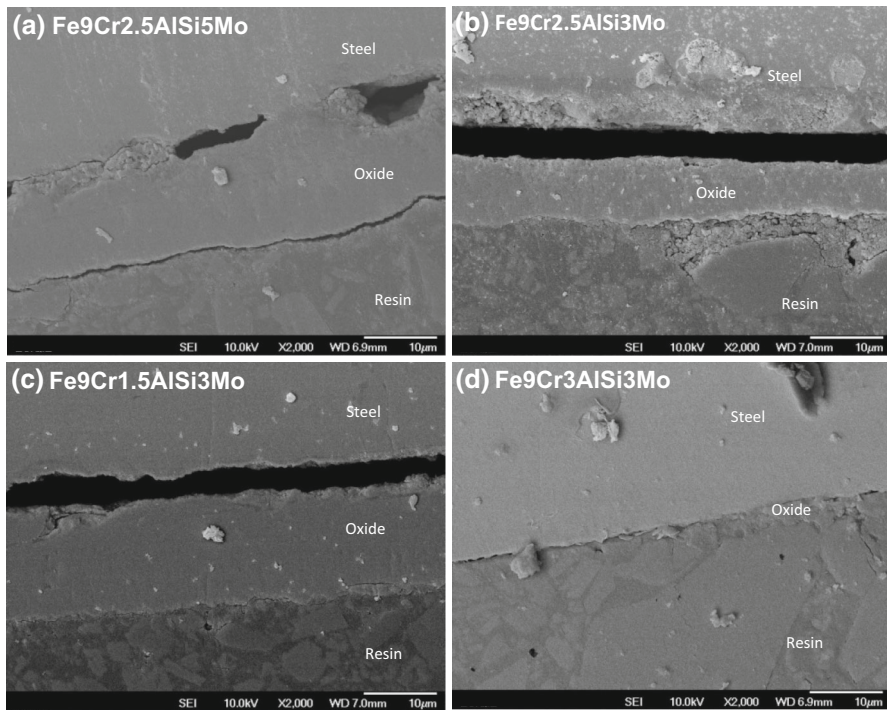
Fig. 8 SEM micrographs of the cross-sections of the alloys corroded after 300 h exposure in N_2–O_2 8 vol% 220 vppm HCl 360 vppm H_2O 200 vppm SO_2 in the presence KCl and ZnCl at 600 °C

Figure 8a–d shows the micrographs for the four alloys tested. These are perpendicular views of the metal surface, here resin refers to the bakelite were the specimen were supported. In Fig. 8a for the alloy Fe9Cr2.5AlSi5Mo, a heterogeneous scale can be observed. The scale is porous has many holes thorough the metal base which are active sites that promote the corrosion. In contrast in Fig. 8b the oxide scale is nearly constant; although the scale looks homogeneous and with a constant thickness, the darkness shadow zone indicates that the scale is not in contact with the metal base; reason why, this oxide is not protective. In Fig. 8c a thicker oxide scale can be appreciated providing a lightly better corrosion protection; but the gap between the metal base and the oxide remains. Finally in Fig. 8d there is no an oxide scale, then the metal base surface remains in contact with the external environmental. In these figures the scale thickness is between 4 and 15 μm. Generally is porous and without a good adhesion to the surface. Moreover notorious gaps between the oxide scale and the base metal are observed. This fact is probably due to the formation of an oxide with two different features: very porous inner oxide and then growing a compact external oxide. This description is similar to the growth mechanism called double film scale [9]. In some cases, fails to observe significant oxide scale because, it is known that the temperature increment will also increase the size of the scale.
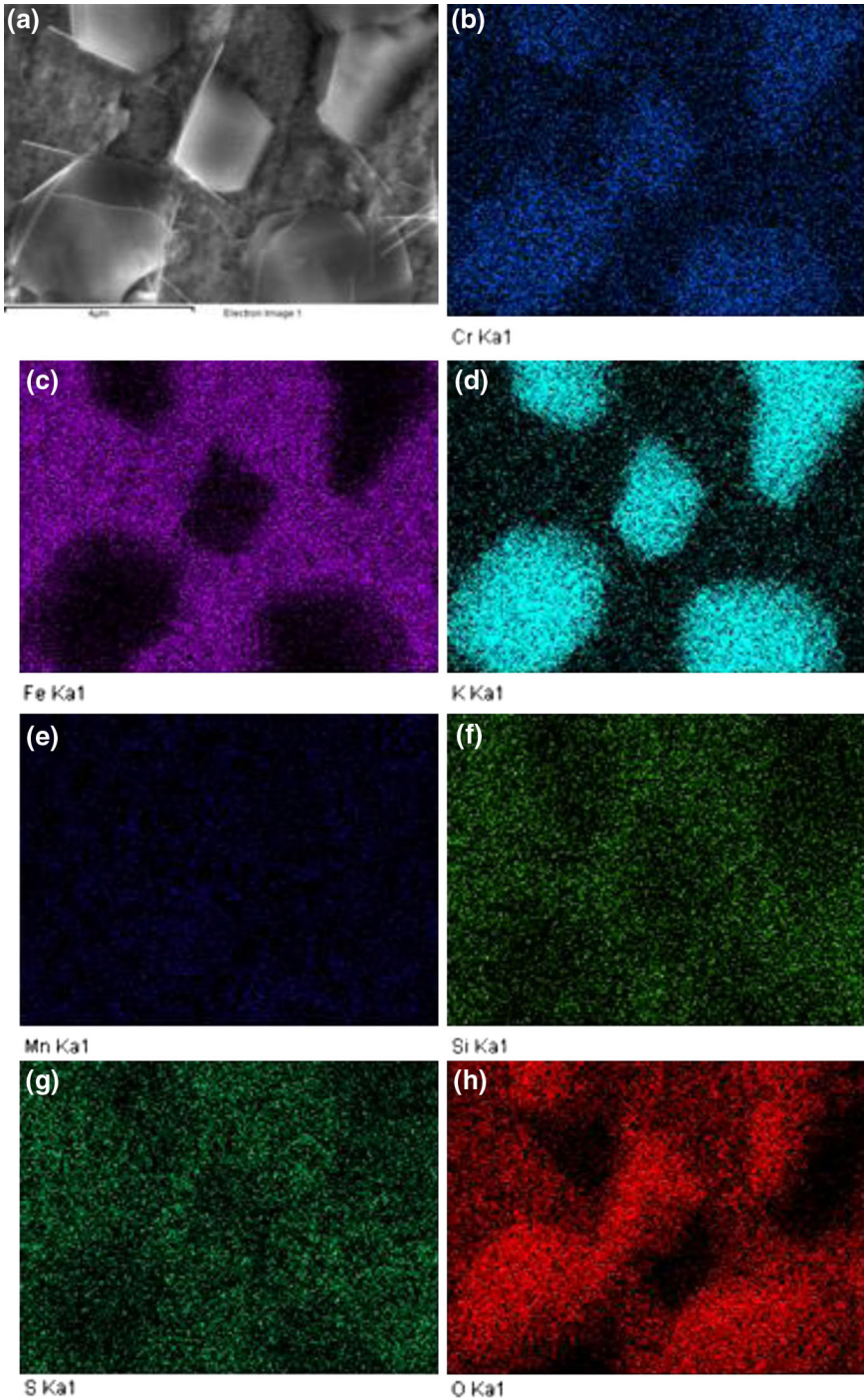
Furthermore in both EDX and SEM analyzes the iron oxide scales were evidenced as a no protective oxides in concordance with previous studies [10–12]. Nevertheless chromium oxides were also found, these are very hard and adhesive products that protect the metal surface.

Figure 9a–h shows a region of the alloy Fe9Cr2.5AlSi5Mo at 600 °C after testing, this specimen was characterized using a surface mapping technique. Figure 9a was taken at ×6000 and corresponds to the original analyzed place in the sample. Here it is possible to observe some precipitates; and the rest of the figures validate the presence of the elements listed below on the rest of the figures. Figure 10a–h represents the same but for the alloy Fe9Cr2.5AlSi3Mo. Here the color intensity evidences the presence of each element.

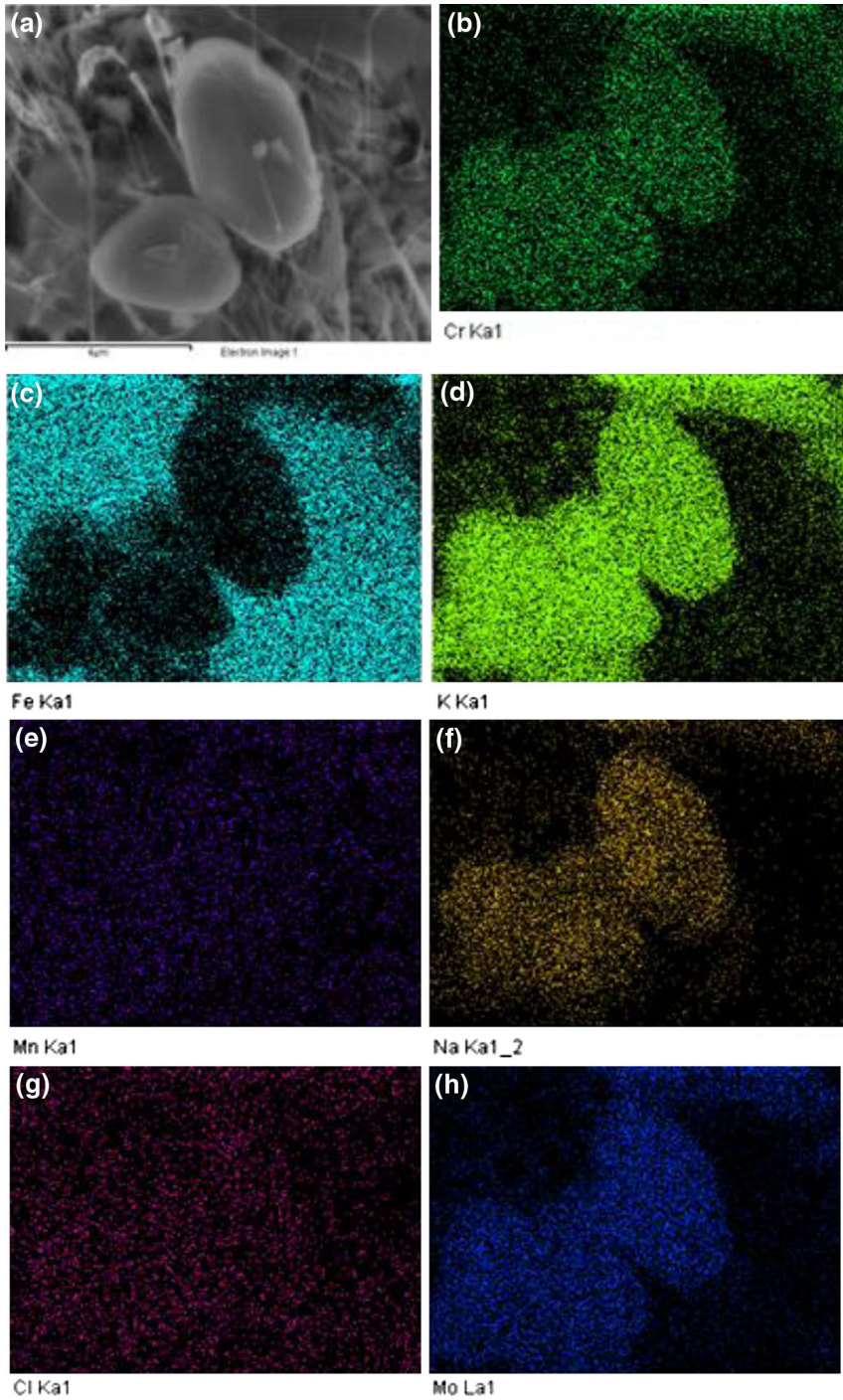## Understanding the Chemical Reactions

The characterization of the products after the corrosion attack shown that the oxide scale formed was porous and with a poor adhesion; thus it was incapable to avoid corrosion on the surfaces. Instead the corrosion process is more intense at 600 °C. The presence of the salts $ZnCl_2$ and KCl is critical due to their fusion temperature is 249 °C; then these are liquid and flows during test; increasing reactivity [13].

The software FactSage 6.3 was used in this research to predict the probable products formation during chemical reactions. The diagram shown in Fig. 11 was obtained for the system corresponding to Fe, Cr and Zn, and the Cl–O–K correspond to chloride, Oxygen and potassium, the metals mentioned represent the alloy chemical composition and the rest the salts in the inlet, both together were used to determine the probable products will be formed and which of them are with the maximum probability to be formed. According with the operating conditions inside the reactor, the diamond in the upper right in Fig. 11 indicates that the $ZnO_{(s)}$, $K_2CrO_{4(s)}$ and $Fe_2O_{3(s)}$ are the most possible products to be formed, this fact was validated with the results obtained from the mapping surface using SEM and also lightly detected during DRX analysis.

The software FactSage 6.3 was used again to predict the chemical behavior at 600 °C; the resulted diagram is shown in Fig. 12. Here Zn(s) and FeO appear as new probable products; moreover the geometry of the diagram in some regions changes, modifying the partial pressures where each product can be formed. But these are far away from our experimental zone; here the most probable products to be formed are again $ZnO_{(s)}$, $K_2CrO_{4(s)}$ and $Fe_2O_{3(s)}$. These products are obtained from the reaction on Eqs. 1 and 2 [14] as follow:

$$Cr + 2KCl_{(g,s)} + 2O_2 \rightarrow K_2CrO_4 + Cl_2 \tag{1}$$
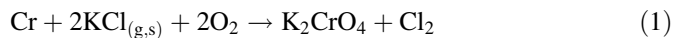
◀ **Fig. 9** Surface mapping of the alloy Fe9Cr2.5AlSi5Mo after 300 h in N_2–O_2 8 vol% 220 vppm HCl 360 vppm H_2O 200 vppm SO_2 in the presence ZnCl2 and KCl at 600 °C

(a) Electron Image 1

(b) Cr Ka1

(c) Fe Ka1

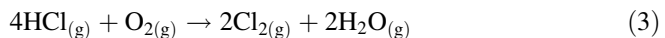(d) K Ka1

(e) Mn Ka1

(f) Na Ka1_2

(g) Cl Ka1

(h) Mo La1
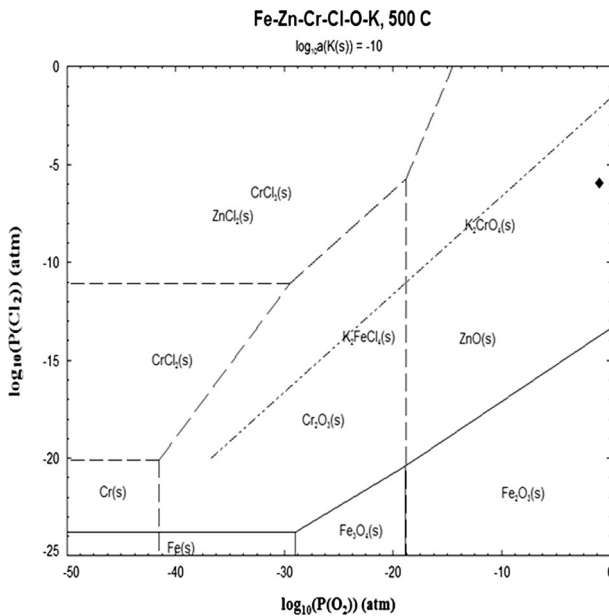
Fig. 11 Superimposed stability diagram system (Fe–Cl–O–K) in *solid lines*, (Zn–Cl–O–K) in *dashed lines*, (Cr–Cl–O–K) in *dot lines* at 500 °C

$$K_2CrO_4 + Cr + Cl_2 \rightarrow Cr_2O_3 + 2KCl + 1/2O_2 \tag{2}$$
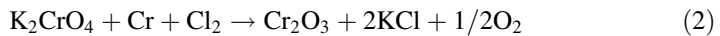
The reaction between metallic chromium and KCl is more probable than between Cr$_2$O$_3$ and KCl in concordance with other authors [15]. In previous studies, initially chromium in the metal base reacts with the oxygen and the salts in the inlet; then potassium chromate and free chloride are produced, but these products became as initiators due to the chemical reaction continues forming the chromium oxide and potassium chloride.
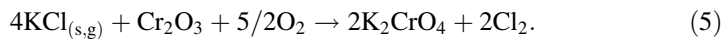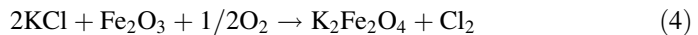
In the other hand the influence of the oxygen and chloride pressure can be exposed as a function of the decomposition of the HCl forming water and the reaction with the metal base in order to obtain K$_2$CrO$_4$ and 2Cl$_2$ again; as is detailed in Eqs. 3–5; but here K$_2$Fe$_2$O$_4$ is formed as an intermediate unstable product which is transformed in the final products indicated in Eq. 2. Here, chloride is driven through cracks and pores in the oxide scale until takes contact with the metal base and forms metallic chlorides. Which are volatile products that remove the weakly stickled oxide scale [14].

$$4HCl_{(g)} + O_{2(g)} \rightarrow 2Cl_{2(g)} + 2H_2O_{(g)} \tag{3}$$
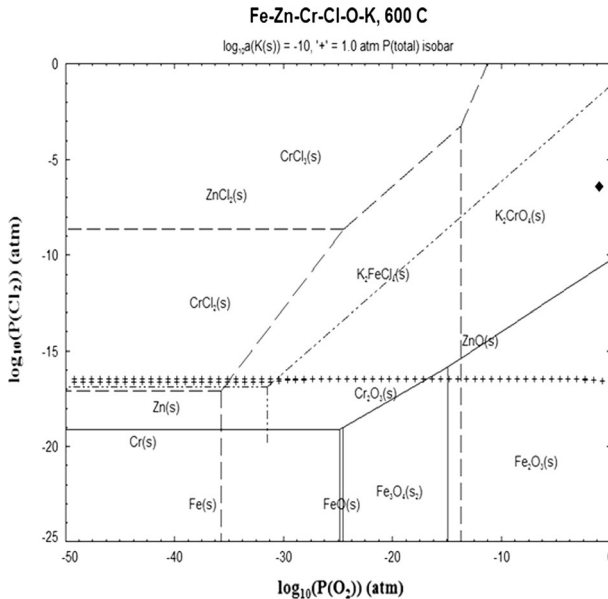
Fig. 12 Superimposed stability diagram system (Fe–Cl–O–K) in *solid lines*, (Zn–Cl–O–K) in *dashed lines*, (Cr–Cl–O–K) in *dot lines* at 600 °C

$$2KCl + Fe_2O_3 + 1/2O_2 \rightarrow K_2Fe_2O_4 + Cl_2 \tag{4}$$

$$4KCl_{(s,g)} + Cr_2O_3 + 5/2O_2 \rightarrow 2K_2CrO_4 + 2Cl_2. \tag{5}$$

Conclusions

There is no evidence of reactivity of the Mo, Si and Al in the four alloys tested.

The only protective oxide formed during testing was Cr_2O_3.

Many of the products formed during the corrosion test were weak and porous oxides which not provide a good protection against corrosion. Oxide layers were not strong enough and allowed the chemical interaction between the metal base and the aggressive environments. Moreover a gap between these, were also found.

Cr was the most active element due to it is in a big amount and because its high free energy.

Cr and Fe formed many intermediate and final products but the chemical products characterized were in concordance with those predicted software FactSage 6.3.

The increments on temperature also increment the mass loss for the alloys Fe9Cr2.5AlSi5Mo and Fe9Cr2.5AlSi3Mo; nevertheless a moderate decrement was observed for alloys Fe9Cr1.5AlSi3Mo and Fe9Cr3AlSi3Mo.

The alloy with the best performance was the alloy Fe9Cr3AlSi3Mo at 600 °C. Although the oxide layer was very thin the mass loss was minor for this alloy.

The whiskers formation evidence the oxide formation in alloys Fe9Cr2.5Al-Si3Mo and Fe9Cr1.5AlSi3Mo, oxide scale appeared formed after nucleation and growth process, although it was consolidated in some micrographs, it was also removed due to its poor adhesive features.

References

1. M. Spiegel, *Materials Science Forum* **971**, 369 (2001).
2. E. Reese and H. J. Grabke, *Materials and Corrosion* **43**, 547 (1992).
3. E. Reese and H. J. Grabke, *Materials and Corrosion* **44**, 41 (1993).
4. T. Jonsson, et al., *Oxidation Metal* **72**, 213 (2009).
5. M. Spiegel, *Materials and Corrosion* **51**, (5), 303 (2000).
6. L.-G. Johansson, et al., Critical Corrosion Phenomena on Super-heaters in Biomass and Waste-Fired Boilers. In *Proceedings of Sino-Swedish Structural Materials Symposium* (2007), pp. 35–39.
7. Y. Kawahara, H. Hagiwara, M. Nakamura, E. Shibuya, and K. Yukawa, Paper No. 564, *CORROSIONl95* (NACE International, Houston, TX, 1995).
8. M. Sánchez-Pastén and M. Spiegel, *Materials and Corrosion* **57**, (2), 192 (2006).
9. M. Danielewski, *Gaseous Corrosion Mechanisms, Corrosion: Fundamentals, Testing, and Protection, ASM Handbook*, vol. 13A, (ASM International, Materials Park, 2003), pp. 106–114.
10. J. Pettersson, et al., *Oxidation of Metals* **72**, 159 (2009).
11. S. Karlsson, et al., *Oxidation of Metals* **78**, 83 (2012).
12. Andreas Ruh and Michael Spiegel, *Corrosion Science* **48**, 679 (2006).
13. W. M. Lu, T. J. Pan and Y. N. Zhang, *Corrosion Science* **50**, 1900 (2008).
14. Y. S. Li, et al., *Corrosion Science* **49**, 1799 (2007).
15. Y. S. Li, et al., *Materials Chemistry and Physics* **93**, 217 (2005).